Journal of
Ceramic Science
and Technology

J. Ceram. Sci. Tech., **05** [04] 281-286 (2014)
DOI: 10.4416/JCST2014-00022
available online at: http://www.ceramic-science.com

CO_2-Laser-Assisted Surface Modification of Titanium Alloys for Biomedical Applications

S. Gräf* **and F. A. Müller**

Friedrich-Schiller-University of Jena, Otto-Schott-Institute of Materials Research (OSIM), Löbdergraben 32, 07743 Jena, Germany

received June 24, 2014; received in revised form August 5, 2014; accepted August 23, 2014

Abstract

The surface of Ti_6Al_4V alloys was activated by means of selective laser microstructuring and subsequent sintering of hydroxyapatite (HAp) nanopowders into the generated structures. For structuring, a novel Q-switched CO_2 laser with pulse durations of about 400 ns and a peak power of up to 7 kW was used. This laser system provides defined blind-holes with structural sizes in the range of 100 – 500 µm. The influence of different process gases (Ar, O_2, N_2) on the formation of titanium oxide (TiO_2) and titanium nitride (TiN) interfaces during laser structuring was investigated with glow discharge optical emission spectroscopy (GDOES). HAp nanopowders prepared via a wet-chemical synthesis route were subsequently sintered into the generated structures using a CO_2 laser with continuous radiation intensities up to 240 W/cm². The homogeneously sintered structures consist of HAp as the major phase and minor amounts of tricalcium phosphate (TCP) and tetracalcium phosphate (TTCP). The formation of TCP and TTCP during laser sintering can be minimized by adjusting sintering parameters (time, laser intensity) and by applying additional process gases (O_2, Ar).

Keywords: CO_2-laser surface structuring, titanium alloy, bioactivation, laser sintering, hydroxyapatite

I. Introduction

Titanium and its alloys are widely used materials for orthopaedic and dental implants owing to their favourable mechanical properties and biocompatibility [1]. However, their Young's modulus significantly exceeds that of human bone, causing undesired stress-shielding effects. Beyond that, titanium and its alloys are classified as bioinert materials. This means that the bone does not substantially bond to the implant. The bioactivity of titanium implants can be enhanced by coating them with a bioactive ceramic, e.g. hydroxyapatite (HAp) [2]. Plasma-spraying techniques are most commonly used to prepare HAp coatings [3]. However, they are typically characterised by an inhomogeneous composition owing to the high processing temperatures and a high risk of crack formation and delamination [2,3].

The objective of the present study was therefore a well-defined partial bioactivation of the surface of the titanium alloy Ti_6Al_4V based on precise laser microstructuring and subsequent sintering of HAp into the generated structures. The great potential of lasers in materials processing (e.g. drilling, cutting, welding) has been demonstrated for all classes of materials [4–6]. However, thermal laser processing of titanium and its alloys is complicated by their low heat conductivity and their high reactivity with oxygen [7–9]. For this reason we used a novel Q-switched CO_2 laser (QPL) [10] for laser structuring. Owing to the operating principle of this laser, the emitted laser pulses are characterised by a pulse duration τ_{imp} of about 400 ns and a peak power P_{max} of about 7 kW, enabling a high-precision ablation process of Ti_6Al_4V. Subsequently, HAp nanopowders prepared based on a wet-chemical synthesis route were sintered into the generated structures using another CO_2 laser with continuous radiation intensities up to 240 W/cm².

The surface of the laser-structured specimen was investigated by means of optical microscopy, tactile surface profilometry and glow discharge optical emission spectroscopy (GDOES). The properties of the sintered specimen were analysed in dependence on the laser intensity and the sintering time using scanning electron microscopy (SEM) and x-ray diffraction measurements (XRD).

II. Experimental Procedure

(1) Laser surface structuring

Fig. 1a schematically illustrates the principle of the experimental setup used for preparation of blind-holes into 4-mm-thick sheets of Ti_6Al_4V (Enpar, Germany). The utilised QPL (µ-storm, IAI, Netherlands) operates in a pulsed pumping mode, leading to the emission of bursts with a repetition frequency f_{rep} = 500 Hz and a duration of 0.5 ms (Fig. 1b). Owing to a rotating chopper disc inside the laser cavity, each burst consists of ten equally spaced single laser pulses with τ_{imp} = 400 ns and P_{max} = 7 kW.

* Corresponding author: stephan.graef@uni-jena.de

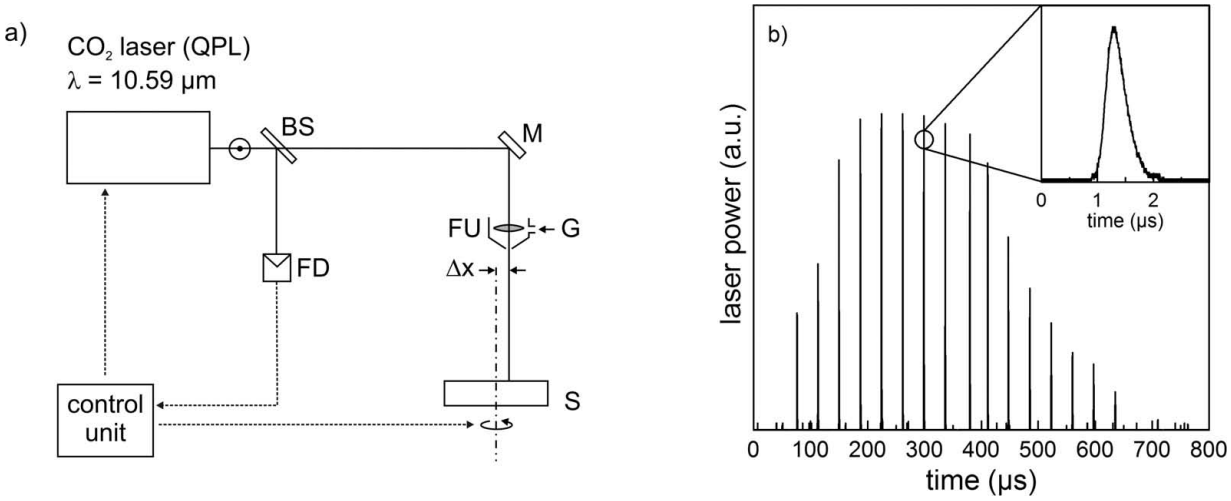

Fig. 1: Principle of the experimental setup [BS: beam splitter, FD: fast detector, M: mirror, FU: focussing unit, G: processing gas, S: sample] and b) laser burst emitted by the QPL.

The linearly polarized radiation of the QPL (wavelength $\lambda = 10.59$ µm, mode quality $M^2 < 1.25$) was focussed onto the sample surface by a focusing unit (FU) containing a zinc selenide meniscus lens (focal length: 1.5", F-number: 1.9) to a focal spot size of about 100 µm. The laser beam parameters were observed with a fast detector (FD) analysing a small part of the radiation reflected by a beam splitter (BS). The blind-holes with a diameter of about 400 µm were realised with a CO_2 laser trepanning process. For this purpose the sample was rotated with a frequency of 500 rpm while the utilised laser beam was kept stationary. The hole diameter was adjusted by means of an additional lateral movement Δx between the rotational axis and the optical axis of the laser beam (Fig. 1a). The velocity of the relative line movement was set to 1 mm/s. Argon (grade: 4.6, purity: 99.996 %), oxygen (grade: 3.5, purity: 99.95 %) and nitrogen (grade: 5.0, purity: 99.999 %) were coaxially applied as processing gas (G) with a pressure of 0.5 bar. For GDOES measurements, flat Ti_6Al_4V reference samples were prepared with an adequate surface polishing procedure and subsequent structuring of an (4x4) mm^2 area. This ablation process was realised by means of bidirectional scanning of the specimen with the QPL radiation and a velocity of v = 1 mm/s. The scanning line spacing was set to 50 µm resulting in a line overlapping of about 50 % of the focal spot size.

(2) Preparation of HAp nanoparticles.

HAp nanoparticles with a molar Ca/P ratio of 1.67 were prepared by means of wet-chemical synthesis using calcium nitrate tetrahydrate, diammonium hydrogen phosphate and ammonium hydroxide. The resulting precipitate was matured for 5 h at 100 °C, and the powders were subsequently dried at 70 °C for 24 h.

(3) CO_2 laser sintering

The HAp nanoparticles were dispersed in acetone and filled into the laser-generated holes. After drying, the powder was first pressed with a needle in the lower part of the structures and finally with stamp-like tool to enhance compaction and to ensure complete filling of the structures (Fig. 2). First experiments to evaluate the sintering behaviour of HAp into Ti_6Al_4V were conducted at the laser-generated blind-holes utilising a commercial CO_2 laser (SM1200P, FEHA Halle, Germany) as radiation source. The sintering intensity I_S and the duration t_S were varied up to 240 W/cm^2 and 20 s, respectively.

Owing to the small size of the laser-generated blind-holes the obtained XRD signal is insufficient for an analysis of the chemical composition of the sintered HAp. Therefore, mechanically manufactured reference holes with diameters of 5 mm and depths of 0.3 mm were used. For a transferability of the results, I_S was kept constant by adjustment of the laser power and the focal spot size to the larger diameter of the holes.

In addition to the sintering process at normal atmosphere (without additional process gas), argon (grade: 4.6, purity: 99.996 %) and oxygen (grade: 3.5, purity: 99.95 %) were applied coaxially to the laser beam into the interaction zone with a pressure of 0.5 bar each.

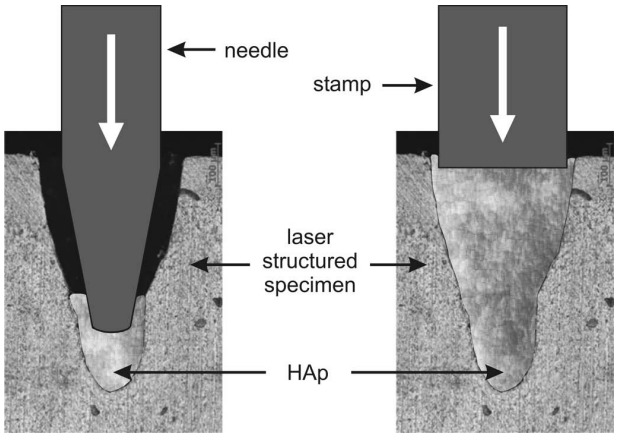

Fig. 2: Filling procedure of the laser-generated blind-holes with HAp nanoparticles.

(4) Characterisation

The surface of laser-structured samples was characterised by means of optical microscopy (VHX-100K, Keyence, Japan) and SEM (S440i, Leica, Germany). The surface roughness was measured with a tactile surface profiling system (Form Talysurf Series 2, Taylor Hob-

son, England). The chemical composition of the surface after laser treatment in dependence on the applied gas atmosphere was analysed with GDEOS measurements. The phase composition and microstructure of the HAp nanoparticles before and after laser sintering were evaluated by means of XRD (D8 Discover, Bruker, Germany) using CuKα radiation (λ= 1.5418 Å) and SEM, respectively.

III. Results and Discussion

(1) Laser structuring

Fig. 3 shows the top view (Fig. 3a) and the cross-sectional view (Fig. 3b) of a blind-hole trepanned into Ti_6Al_4V using the QPL and oxygen (p = 0.5 bar) as process gas. The entrance diameter is about 400 µm and can be adjusted to arbitrary values exceeding 100 µm by means of an appropriate relative movement rx during the trepanning procedure (see Fig. 1a). The shape of the holes is conical, resulting in a depth of about 560 µm.

The micrographs shown in Fig. 3 confirm a high-precision CO_2 laser ablation process, which results from the short pulse duration of the QPL pulses. In addition to the material-specific thermal diffusivity the thermal diffusion caused by heat conduction strongly depends on the interaction time of the radiation with the material (i.e. the pulse duration τ_{imp}). Consequently, the energy transport from the erosion front into the bulk material decreases with decreasing τ_{imp}, which results in a reduced melt formation.

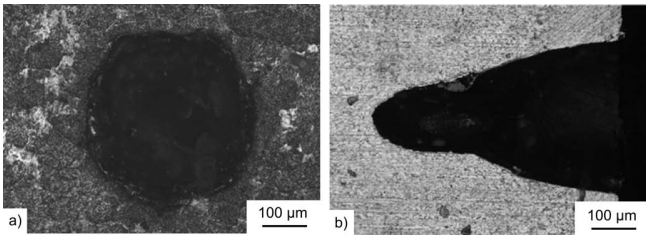

Fig. 3: Optical micrographs of a) the top surface and b) the cross-section of a blind-hole trepanned into Ti_6Al_4V with the QPL and O_2 as processing gas (p = 0.5 bar).

Fig. 4 shows sections from flat Ti_6Al_4V surfaces (4 x 4 mm^2) structured with the QPL pulses using Ar (Fig. 4a), N_2 (Fig. 4b) and O_2 (Fig. 4c) as process gases (p = 0.5 bar). The obtained surface structure results from the hemispherical geometry of the single-pulse ablation process that is modified by the overlap of adjacent laser pulses in moving direction and the scanning line spacing. The corresponding average surface roughness was measured to R_a = 3.892 µm (Ar), R_a = 3.187 µm (N_2) and R_a = 2.916 µm (O_2). Owing to the strong exothermal reaction of heated and melted Ti_6Al_4V, laser structuring with O_2 results in the highest ablation rate of all applied gases.

As illustrated in Fig. 4, the surfaces reveal different colours after laser structuring with different process gases. This visual impression indicates the formation of different types of surface layers. The specimen structured with Ar (Fig. 4a) retained its metallic brilliance as expected from other laser materials processes like welding where Ar acts as a shielding gas and prevents chemical reactions of the heated material with the surrounding atmosphere [11]. In agreement with the results reported by Selamat *et al.* [12]. the use of N_2 (Fig. 4b) results in a golden-coloured surface suggesting the appearance of titanium nitride (TiN). The surface structured with O_2 is coloured black (Fig. 4c), which might be related to the exothermal oxidation of Ti_6Al_4V and the formation of titanium oxide (TiO_2).

Fig. 5 shows the analysis of the chemical composition of the laser-structured surfaces obtained from GDOES-measurements. The graphs show the relative intensity of the elements oxygen (Fig. 5a) and nitrogen (Fig. 5b) in dependence on the time of analysis, i.e. the sputter time. This time corresponds to the investigated material's depth. For the purpose of greater clarity, the elements titanium, aluminium and vanadium are not displayed. But it should be mentioned that after an adequate sputter time the relative intensities of oxygen and nitrogen tend to zero and the chemical composition expected for the Ti_6Al_4V bulk material arises. It is evident from Fig. 5 that Ar acts as a shielding gas, which prevents chemical reactions of the heated and melted metal with the surrounding atmosphere. The time dependence of the relative intensity obtained from the specimen structured with Ar equals that of the untreated bulk material. The increased relative intensity of oxygen at the beginning of the measurement in both curves results from the very stable passive layer of several nm thickness that is instantly formed when the metal is exposed to air [13]. Contrary to this, the specimen structured with O_2 reveals a remarkable increase of the oxygen content also in deeper regions of the bulk material. This indicates the formation of a laser-induced TiO_2 layer. On the other hand, a significant amount of nitrogen can be detected at the Ti_6Al_4V surface after structuring with N_2, indicating the formation of TiN.

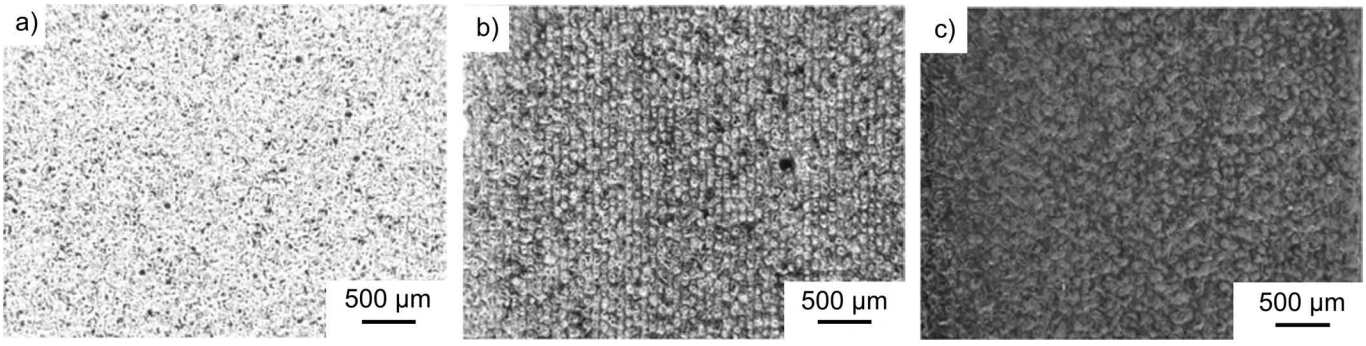

Fig. 4: Optical micrographs of Ti_6Al_4V surfaces structured with the QPL using a) Ar, b) N_2 and c) O_2 as process gases (p = 0.5 bar).

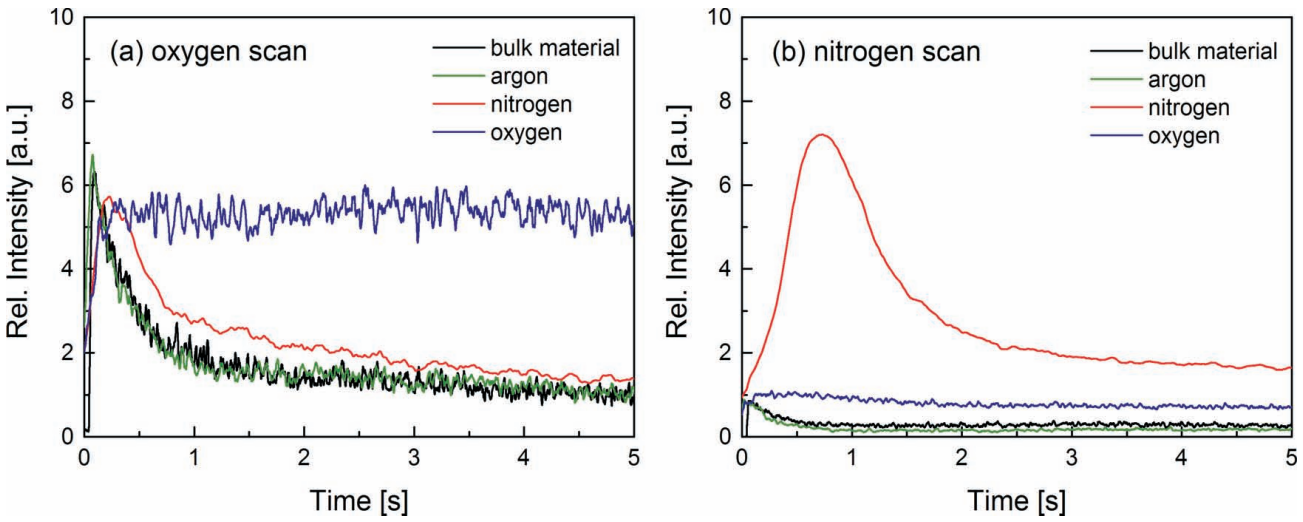

Fig. 5: GDOES-scan for a) oxygen and b) nitrogen of Ti_6Al_4V surfaces structured with the QPL using Ar, N_2 and O_2 as process gases.

The formation of the ceramic oxide and nitride layers can be explained by the increased chemical reactivity of the heated and molten material with the surrounding atmosphere. But, melt formation and chemical reactions are localised to the direct vicinity of the focus as a consequence of the short pulse duration. This molten material is resolidified immediately after the ablation process, whereas crack formation in the layers is not observable. The obtained results demonstrate that well-defined intermediate layers can be generated *in situ* as bond coats during CO_2 laser structuring with an adequate process gas.

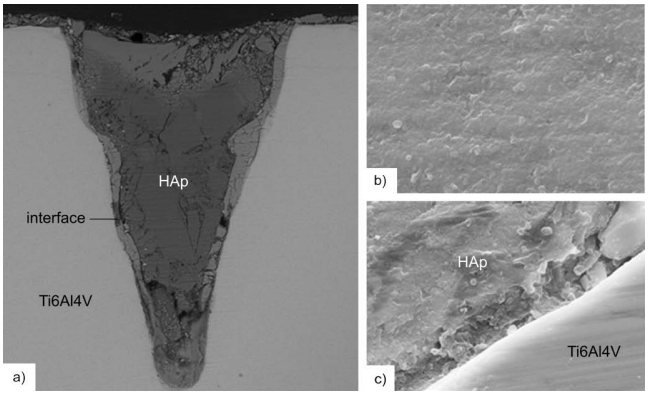

Fig. 6: SEM micrographs of a blind-hole sintered with I_S = 120 W/cm² and t_S = 20 s; a) cross-section, b) magnified central region and c) magnified interface between HAp and Ti_6Al_4V.

(2) Sintering of HAp into Ti_6Al_4V surfaces

The HAp nanoparticles were filled into the laser-generated structures and sintered at different laser intensities and sintering times. Fig. 6 shows a SEM micrograph obtained from a cross-section of a blind-hole after sintering with I_S = 120 W/cm² and t_s = 20 s. As labelled in this micrograph, three different regions can be evaluated: the untreated titanium alloy (bright area), the interface next to the bulk material resulting from the thermal ablation process and the laser-sintered HAp (dark area). A larger magnification of the centre region (Fig. 6b) confirms a densely sintered HAp structure. Moreover, Fig. 6c illustrates that a close connection at the interface between HAp and Ti_6Al_4V occurs after sintering. Nevertheless, Fig. 6a reveals an incomplete densification in the upper part of the cross-section, which might result from an insufficient compaction of the powder before sintering (see Fig. 2).

The chemical composition of HAp was investigated before and after laser sintering without an additional process gas using XRD. In Fig. 7a, I_S was varied from 80 to 240 W/cm² at constant t_s = 5 s. In Fig. 7b, I_s was kept constant at 120 W/cm² and t_s was varied between 5 and 20 s. In both graphs the peaks appearing for the initial HAp powder (lower curves) match the typical peaks for HAp (JCPDS 74 – 566). They are indicated in Fig. 7 by the black squares.

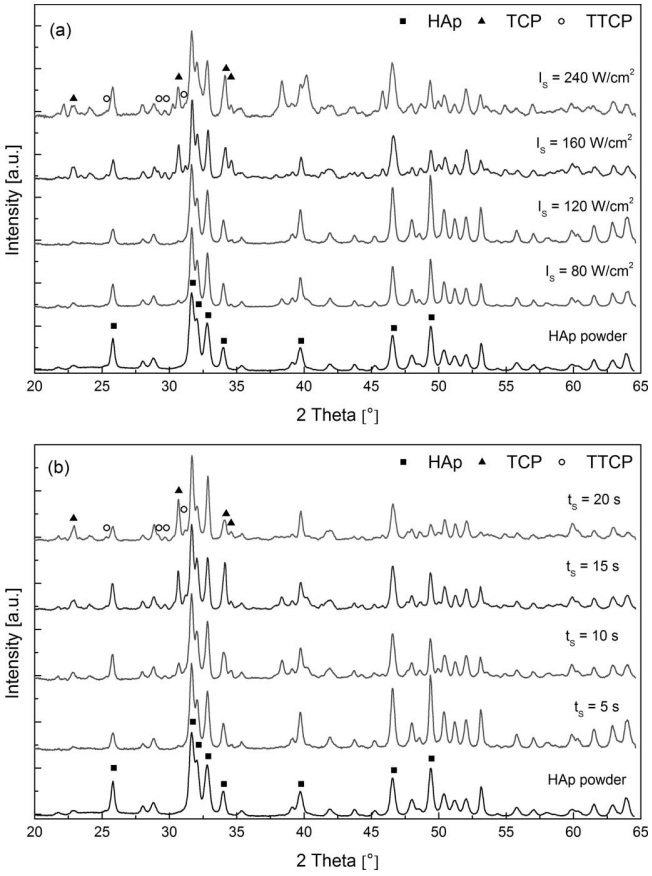

Fig. 7: X-ray diffraction spectra of HAp sintered without additional process gas in dependence on a) I_s and b) t_s.

Up to t_s = 20 s and I_s = 240 W/cm^2, HAp was found to be the major occurring phase. However, with increasing t_s and I_s, peaks associated with tricalcium phosphate (TCP) and tetracalcium phosphate (TTCP) appear in the spectra. These peaks are indicated for the upper curve in each case. According to Zhoy *et al.* [14], their appearance can be explained by a loss of OH groups during the thermal treatment beyond 1200 °C and a transformation to oxyapatite. At 1450 °C the latter dissociates into α-$Ca_3(PO_4)_2$ [TCP], $Ca_2P_2O_7$ [CPP] and $Ca_4P_2O_9$ [TTCP]. This behaviour is also well-known from conventional sintering [14, 15] or plasma spraying [16] of hydroxyapatite. For completeness, the peaks occurring at 2Θ = 38.36° and 2Θ = 40.16° refer to the titanium bulk material.

Fig. 8 shows the influence of an additional process gas (p = 0.5 bar) on the chemical composition of HAp sintered with I_S = 240 W/cm^2 and t_S = 20 s. It becomes evident that when compared with the initial HAp powder and the sintering process without additional process gas, the formation of TCP and TTCP can be reduced remarkably if Ar and O_2 are used.

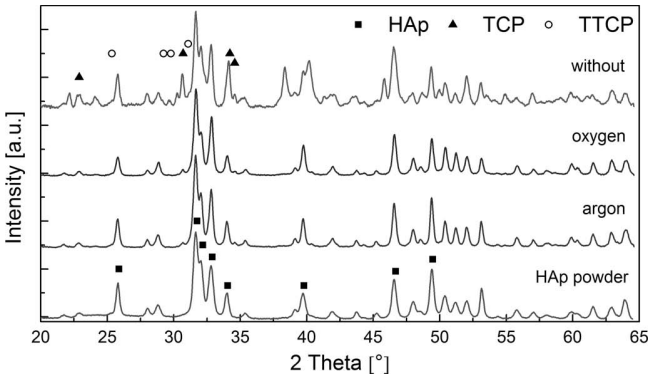

Fig. 8: X-ray diffraction spectra of HAp in dependence on different process gases (p = 0.5 bar).

IV. Conclusions

In this study the surface of Ti_6Al_4V was microstructured using a novel Q-switched CO_2 laser and the process gases O_2, N_2 and Ar. It was shown that the chemical composition of the laser-structured surfaces can be modified specifically. HAp prepared by laser sintering into reference holes showed a homogenous and dense microstructure. A gradual decomposition of HAp into TCP and TTCP was observed with increasing durations of sintering and laser intensities. This decomposition can be reduced by applying adequate additional process gases during sintering.

Acknowledgements

The authors gratefully acknowledge the assistance of Mr Robert Hanke, who performed the GDOES measurements.

References

1 Long, M., Rack, H.J.: Titanium alloys in total joint replacement – a materials science perspective, *Biomaterials*, **19**, 1621 – 1639, (1998).

2 Sun, L.M., Berndt, C.C., Gross, K.A., Kucuk, A.: Material fundamentals and clinical performance of plasma-sprayed hydroxyapatite coatings: A review, *J. Biomed. Mater. Res.*, **58**, 570 – 592, (2001).

3 Narayanan, R., Seshadri, S.K., Kwon, T.Y., Kim, K.H.: Calcium phosphate-based coatings on titanium and its alloys, *J. Biomed. Mater. Res. B*, **85B**, 279 – 299, (2008).

4 Steen, W.M.: Laser material processing, 4th ed., Springer, New York, 2010.

5 Sugioka, K.J., Meunier, M., Piqué, A.: Laser precision microfabrication, Springer, Berlin, 2010.

6 Mordike, B.L.: Lasers in materials processing, *Prog. Mater. Sci.*, **42**, 357 – 372, (1997).

7 Welsch, G., Boyer, R., Collings, E.W.: Materials properties handbook: titanium alloys, ASM International, Materials Park, OH, 1994.

8 Yilbas, B.S., Akhtar, S.S., Karatas, C.: Laser trepanning of a small diameter hole in titanium alloy: temperature and stress fields, *J. Mater. Process. Tech.*, **211**, 1296 – 1304, (2011).

9 Rao, B.T., Kaul, R., Tiwari, P., Nath, A.K.: Inert gas cutting of titanium sheet with pulsed mode CO_2 laser, *Opt. Laser. Eng.*, **43** 1330 – 1348, (2005).

10 Staupendahl, G.: CO_2 laser with rapid power control, IAI INDUSTRIAL SYSTEMS B.V. (De Run 5406, DE Veldhoven, NL-5504, NL) 2013.

11 Akman, E., Demir, A., Canel, T., Sinmazcelik, T.: Laser welding of Ti_6Al_4V titanium alloys, *J. Mater. Process. Tech.*, **209**, 3705 – 3713, (2009).

12 Selamat, M.S., Baker, T.N., Watson, L.M.: Study of the surface layer formed by the laser processing of Ti-6Al-4V alloy in a dilute nitrogen environment, *J. Mater. Process. Tech.*, **113**, 509 – 515, (2001).

13 Donachie, M.J.: Titanium: A technical guide, ASM International, Metals Park, Ohio, 1988.

14 Zhou, J.M., Zhang, X.D., Chen, J.Y., Zeng, S.X., Degroot, K.: High-temperature characteristics of synthetic hydroxyapatite, *J. Mater. Sci. -Mater. M.*, **4**, 83 – 85, (1993).

15 Ramesh, S., Aw, K.L., Tolouei, R., Amiriyan, M., Tan, C.Y., Hamdi, M., Purbolaksono, J., Hassan, M.A., Teng, W.D.: Sintering properties of hydroxyapatite powders prepared using different methods, *Ceram. Int.*, **39**, 111 – 119, (2013).

16 Boch, P., Niepce, J.-C.: Ceramic materials: processes, properties and applications, ISTE USA, Newport Beach, CA, 2006.